Sensitization Towards Aerosol Optical Properties And Radiative Forcing , Real Case In Morocco

Somia SSOUABY[1], Hafida NAIM[1], Abdelouahid Tahiri[2], Salmane BOUREKKADI[3]

[1]Faculty of Sciences, Ibn Tofail University, Kenitra Morocco

[2]Faculty of Sciences, Mohammed First University, Oujda Morocco

[3]University of Poitiers, Poitiers France

Abstract. Mineral dust is one of the most important aerosol components in the Earth's atmosphere. Desert aerosol constitute the main types of tropospheric aerosols whose optical property uncertainties are still quite important. In this study, we analyse the variability of aerosol optical depth (AOD), Angstrôm Exponent (α), Single Scattering Albedo (ω_0) and aerosol radiative forcing (ARF) of desert aerosol recent measurements, for six AERONET sites covering the belt desert areas: Ouarzazate (Morocco), Tamanrasset (Algeria), El Farafra (Egypt), Mezaira (Unites Arab Emirates), Kuwait University (Kuwait), Dalanzadgad (Mongolia). The annual cycle of the aerosol optical depth dialy averages shows variable values due to the changeable weather and the Sahara source. The highests were recorded at the Sahara site (2.2 at Tamanrasset) and (2.9 at Kuwait-University). The spectral single scattering albedo SSA annual averages varies in the interval (0,8-0.95) indicating dominant scattering. Desert aerosol radiative forcing shows always a negative ARF with a maximums registred in July, -90 W/m^2 at surface (Mezaira) and -26 W/m^2 at the top of the atmosphere (Kuwait) that imply a general trend towards regional warming of the total column atmosphere with a maximum near +55 W/m^2 observed in July at UAE.

1 Introduction

The sensitivity of climate models to the characterization of the continents aerosol particles needs more measurements. Africa is a major source of dust and biomass burning aerosols, this represents an important research gap in understanding the impact of aerosols on radiative forcing of the climate system. Mineral dust particles are one of the main constituents of the atmospheric aerosol which influence the radiation budget of the atmosphere. The evaluation of the dust-radiation interaction is essential for climate forcing assessment at both local and regional scales. However, large uncertainties still remain in assessing the dust climate impacts. To determine the radiative effects of dust it is crucial to characterize its optical properties and corresponding PSDs [1]. The Sahara desert is the important source of mineral dust in the Northern Hemisphere, it constitutes the first part of the belt desert area (Fig.1) . North African dust is injected into the atmosphere through resuspension processes at the source areas, and may be transported particularly with dust storms at different altitudes (up to 7km) to different areas in the world [2]. Remote sensing results of dust optical properties indicate that dust is nearly non-absorbing [3], while earlier laboratory measurements suggested dust to be partly absorbing at visible wavelengths [1]. Many measurements campaign in desert zone were conducted in the past, the successful one with SAMUM consortium undertaken on May-June 2006 at Ouarzazate and Zagora (Morocco) close to Sahara gives very important description including chemical and physical properties of desert aerosol near ground and at different altitude levels during its transport [4]. The omnipresence of dust causes a direct radiative forcing, but the magnitude (its sign and its global significance) is always discussed [5]. Saharan desert dust contributes significantly to the global dust burden [6]. Physical properties of the mineral dust as well as its chemical and mineralogical composition and state of mixing modify its influence on climate and atmospheric chemistry [7]. Aerosol optical properties are difficult to characterize globally due to their large spatial and temporal variability. In fact, the short residence times in the atmosphere (days to weeks) and the large variability in composition and particle size distribution (wide range of sources) contribute of both natural (primarily sea salt and desert dust) and anthropogenic (primarily combustion of biomass and fossil fuels) aerosol disseminations.

This study concernes the analysis of recent aerosol optical data obtained from AERONET/PHOTONS (http://aeronet.gsfc.nasa.gov/). The main optical aerosol parameters are: aerosol optical depth AOD at SW 0,5µm, Angstrôm Exponent (α), Single Scattering Albedo (ω_0) and aerosol radiative forcing (ARF) of six sites covering the belt desert areas: Ouarzazate (Morocco), Tamanrasset (Algeria), El Farafra (Egypt), Mezaira (Unites Arab Emirates), Kuwait University (Kuwait) and Dalanzadgad (Mongolia) (Table 1).

2 Climate site descriptions

The six sites are selected in the belt desert regions (Fig.1) and there localisations are presented in Table 1.

- ✓ **Ouarzazate, Morocco**

Ouarzazate is a small town with almost no industrial activity. It is located in the South-East of the Atlas and has a pre-Saharan climate characterized by low rainfall and hot and dry climate, Bsh Köppen classification. The

*Corresponding author: dyourim@gmail.com , somia.souaby@gmail.com

average maximum temperature in July is 40°C, the average minimum is 25°C. in January, the temperature at night can drop to -4°C. In the spring, clouds are rare and exceptional thunderstorms. The desert winds (Sirocco and Chergui) play an important role in the Ouarzazate climate.

✓ **Tamanrasset, Algeria**

This zone does not know any industrial activities and is located in the high platau of the Sahara. The climate of Tamanrasset is warm, sunny, arid and tropical, BWh in Köppen classification. Winter temperatures are close to those of the rest of the Sahara, while the summer maximums are below 35°C, the nights are icy and the days are mild. Tamanrasset is crossed by the Sirocco violent, very dry and very hot Saharan wind that blows over North Africa loaded with burning Saharan air mass. The Harmattan hot, dry and dusty wind of West Africa lows southward from the Sahara and is loaded with dust and sand.

✓ **El Farafra, Egypt**

The station is located outside the village in a flat open desert environment. Qualified as white desert in the northeast of the Sahara, between the Egyptian oases of Al-Farafra in the southwest and Al-Bahariya in the northeast. Its soil is formed of white limestone contrasting with the surrounding ergs of yellow sand.. In this eastern part of the Sahara, the temperature can exceed 45°C in summer. Rain very rarely falls in the year. The desert wind can pick up and create huge sandstorms.

✓ **Mezaira, United Arab Emirates**

With desert climate, characterized by mild winters and very hot, sunny summers, with the humidity of the Persian Gulf that makes the heat unbearable. Annual precipitation is almost everywhere below 100 millimeters and is concentrated in winter. The maximum winter temperatures range from 24°C to 26°C. Summer is very hot and sunny, with daytime temperatures ranging from 38°C to 42°C between May and September, and with the wind from the Persian Gulf that brings moist air from the sea, making the heat sweltering. April and October are also hot months. During the hottest days, the temperature can reach 48 °C on the coast, and even more in the interior. All year round, but especially in spring, the UAE may be affected by strong winds, which can bring dust and sand storms.

✓ **Kuwait-University, Kuwait**

The sun-photometer is placed at the roof top of building in Kuwait University, Khalidiyah Campus. Khalidiyah is an urban area, approximately 4.8 Km from Kuwait city. Hot and dry throughout most of the year, with very little rainfall. The brief winter months bring some mild cooling. Most of Kuwait lands are flat and dry barren desert of the sandy plains.

✓ **Dalanzadgad, Mongolia**

Is located at the top of a platform in southern Mongolia. Due to its high altitude and its remoteness from any sea, it has an extreme continental climate with BSk Köppen classification: very cold winter, with temperatures as high as -30°C, and was short but hot, especially in the Gobi Desert. The sun shines on average 257 days a year, the country being generally at the center of a system of high pressures (anticyclones). It rains very little with an annual average of 250 mm in the North. The extreme south, Gobi desert may not receive rainfall for several years.

Table 1. AERONET/PHOTONS site informations

AERONET Site	Country	Latitude	Longitude	Elevation (Meters)
Ouarzazate	Morocco	30.92837°N	6.91287°W	1136
Tamanrasset	Algeria	22.79000°N	5.53000°E	1377
El Farafra	Egypt	27.05800°N	27.99017°E	92
Mezaira	U. A.Emirates	23.10452°N	53.75466°E	210
Kuwait University	Kuwait	29.32500°N	47.97100°E	42
Dalanzadgad	Mongolia	43.57722°N	104.41917°E	1470

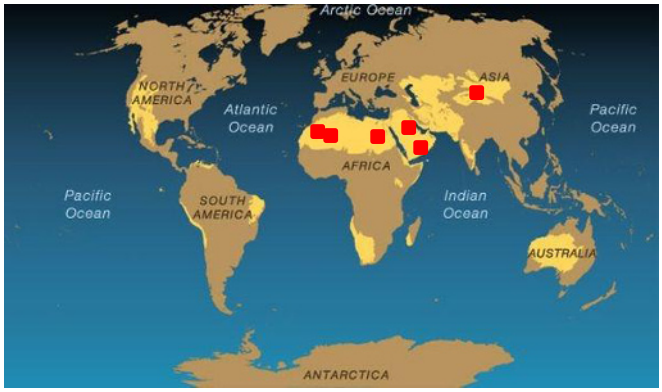

Fig. 1. AERONET/PHOTONS Sites selected in the belt desert area.

3 Instrumentation and method

The AERONET / PHOTONS network was set up by the Goddard Space Flight Center (NASA, USA) and the Atmospheric Optics Laboratory of Lille (CNRS, France) in 2003. Since its creation, it has collected ground measurements by solar photometers to specify the optical and microphysical properties of the atmospheric particles. About 1500 stations spread all over the globe, are currently listed. The instruments of the network are regularly checked and calibrated with an identical protocol. The data are processed in the same way regardless of the date and place of acquisition, whether for the inversion itself [8] or for the rejection of the measurements affected by the presence of clouds [9]. The CIMEL CE-318 solar photometers (Fig.2) are instruments allowing the restitution of the optical and microphysical properties of vertically integrated aerosols of the atmospheric column. Photometric measurements are possible only during the day when the sun is visible and in the absence of clouds. Detailed photometer description is made by B. Holben et al., 1998 [10]. The photometer moves in the zenith and azimuth planes and can aim at any point of the celestial cost with an accuracy of 0.05° and a field of view of 1.2°. It has a filter wheel to measure in eight channels between 0.34

and 1.64 µm (Table 2). These spectral filters with a width of 0.01 µm correspond to atmospheric windows where the absorption of solar radiation by the gaseous compounds is low. The data is transmitted by a geostationary satellite every four hours to a single processing center located at NASA's Goddard Space Flight Center. The photometer provides direct sunlight measurements and scattering measurements according to the angular luminance distribution of the sky ($W/m^2.Sr.\mu m$) in the Almucantar (circle of the same solar elevation including the sun and which forms the base of the half angle cone the constant zenith angle of view θ, (Fig.3). Several sequences of Almucantar measures in average in 35s are carried out morning and afternoon. A sequence of measurements records i measurements along the Almucantar Ai directions on 2π (rd).There are different levels of data processing available: level 1 (raw data), level 1.5 (the cloud mask is automatically applied when the final calibration is not necessarily performed) and level 2 (the cloud mask is applied as well than the final calibration). For our study, the data for levels 1.5 and 2 were used. The algorithm used in AERONET [8] and [11] characterizes aerosols by assimilating luminance simulated by a radiative transfer code with measurements of luminance (direct luminance of the sun and sky luminance) obtained at 4 wavelengths (440, 675, 870 and 1020µm). The use of the radiative transfer code makes it possible to determine by inversion the desired optical properties. Several studies with other radiative transfer codes involving non-linear inversion methods have been carried out [12] and [13] and have allowed the determination of the optical properties of the desert aerosol. The last ones [14] have been proposed for particles of non-spherical shapes.

Table 2. Nominal AERONET wavelengths for ion-assisted deposition filtres used for aerosol remote sensing and spectral corrections or components for each channel.

Wavelengths(nm)	Filter bandpass (nm)	Spectral corrections/components
340	2	Rayleigh, NO_2, O_3
380	2	Rayleigh, NO_2
440	10	Rayleigh, NO_2
500	10	Rayleigh, NO_2, O_3
675	10	Rayleigh, O_3
870	10	Rayleigh
935	10	Rayleigh, aerosol
1020	10	Rayleigh, H_2O
1640	25	Rayleigh, H_2O, CO_2, CH_4

Fig.2. Sample images of the sun photometers CIMEL CE- 318 installed at El Farafra and Mezaira sites

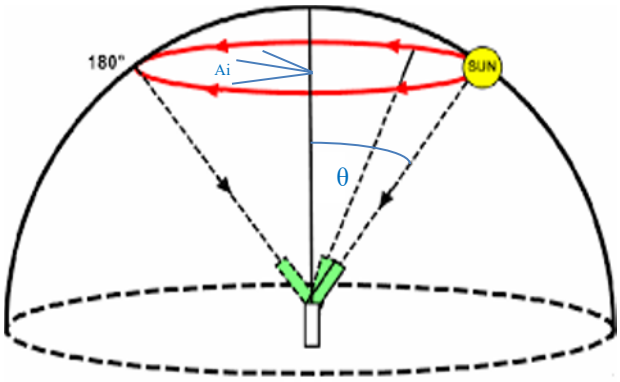

Fig.3. Sample Almucantar positions of the photometer.

4 Results and discussion

4.1 Aerosol Optical Depth and Angstrom Exponent

Aerosols are small solid or liquid particles suspended in the atmosphere. They come from natural or anthropogenic sources and their size can vary from nanometer (groups of molecules) to a few tens of micrometers (dust particles). Since the industrial revolution, man began to emit massively aerosols. Sun photometry is a passive remote-sensing measurement technique in which mainly collimated light generally not scattered or absorbed by the atmosphere illuminates a photodiode detector and this light energy is converted to a digital signal (V) [15], [16] and [17] . The Beer-Lambert-Bouguer law converted to instrument digital counts is shown in Eq. (1):

$$V(\lambda) = V_0(\lambda).d^2.exp[-\tau(\lambda).m] \qquad (1)$$

where V(λ) is the measured spectral voltage of the instrument dependent on the wavelength λ, $V_o(\lambda)$ is the relative extraterrestrial spectral calibration coefficient dependent on λ, d is the ratio of the average to the actual Earth-Sun distance [18], τ(λ) is the total optical depth, and m is the optical air mass, which is strongly dependent on the secant of the solar zenith angle [19].

The spectral AOD ($\tau(\lambda)_{Aerosol}$) should be computed from the cloud-free spectral total optical depth $\tau(\lambda)$ and the subtraction of the contributions of Rayleigh scattering optical depth $\tau(\lambda)_{Rayleigh}$ and spectrally dependent atmospheric trace gases absorption optical depth $\tau(\lambda)_{Abs}$ as shown in Eq. (2).

$$\tau(\lambda)_{Aerosol} = \tau(\lambda) - \tau(\lambda)_{Rayleigh} - \tau(\lambda)_{Abs} \qquad (2)$$

Where $\tau(\lambda)_{Abs}$ is the sum of the optical depth of ozone O_3, the nitrogen dioxide NO_2, the water vapor H_2O, the carbon dioxide CO_2 and the methane CH_4 calculated based on the assumptions defined in Holben et al. (1998) [17], and assuming the US standard atmosphere (1976) and absorption constants derived from HITRAN [18], [19], [20] and [21].

The annual cycle of daily averages of AOD at 0.5µm and the corresponding Angstrom Exponent determined at 0.44-0.87µm relative to the six sites are presented in Fig.4. In **Ouarzazate** (Fig.4.a), peaks are recorded in spring and summer. The maximum reaches 1.4. The aerosol type changes alternately in the Ouarzazate region because of the low influence associated with the Atlantic air masses which moderate the dust load of the East and Saharan air masses on summer. Minimums are recorded in the fall and winter [23]. The daily average is 0.28 in agreement with the SAMUM experimental measurement campaign carried out in May-June 2006 in Ouarzazate, [24,25]. The Angstrom coefficients show that the largest values of the aerosol optical depth are associated with small α characteristic of the presence of desert dust in summer coming mainly from the Southeast [23]. At **Tamanrasset** (Fig.4.b), we observe strong variability recorded for the large values (from March to September) with a maximum of 2.2. Very high values are characteristic of the Saharan aerosol charge. Similar results have been reported by Kim et al. [26, 27] with analysis limited to the properties of dust aerosols with data (AOD ≥ 0.4) and Angstrom coefficients less than 0.2. The **El Farafra** site (Fig.4.c) records relative high AODs with a maximum (~ 1.2) in March due to the influence of the white desert (desert of stones). In **Mezaira** (Fig.4.d), peaks are recorded in spring and summer, with a maximum in July (~ 1.2) due to the strong winds, which can bring dust and sand storms. **Kuwait-University** (Fig.4.e) shows significant variability of large AODs (March to September) with the respective maximum of 2.9, that confirm the importance of the desert aerosol in summer and lesser degree in spring. At **Dalanzadgad** (Fig.4.f), AODs show significant variations throughout the year, characteristics of submicron particles. the annual cycle records values below 0.2, these low AODs are due to the diversity of the landscapes of the Dalanzadgad which consists of vast plains, imposing mountain ranges and dunes, as well as saline steppe areas. Rare peaks near 0.6 are observed in March-April-May may be explain by the influence of the sand dunes of the Gobi Desert which is located between northern China and southern Mongolia.

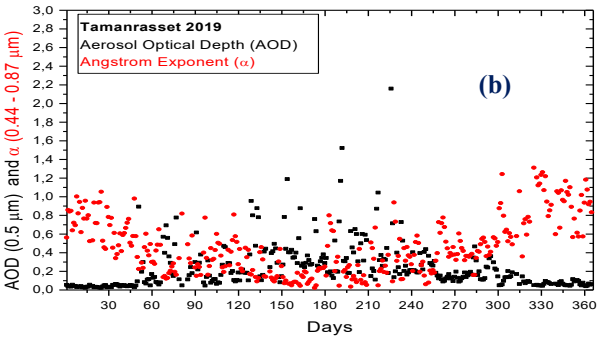

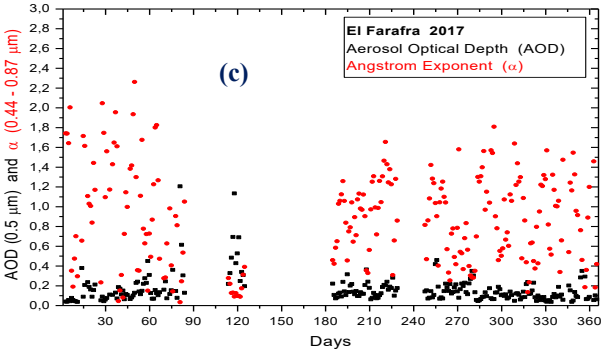

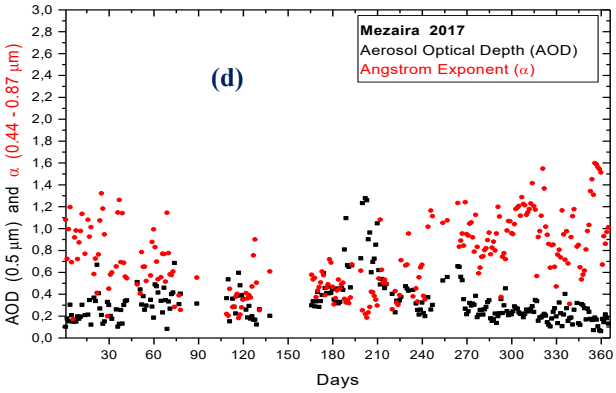

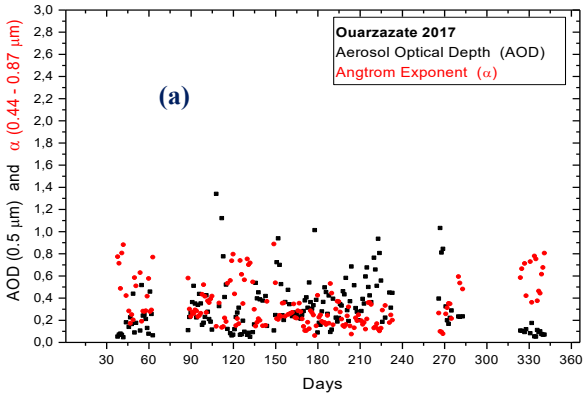

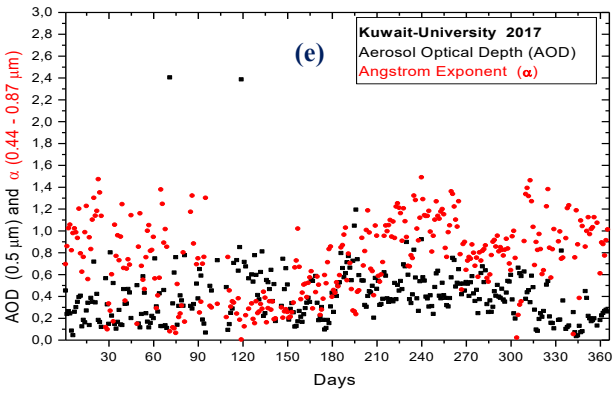

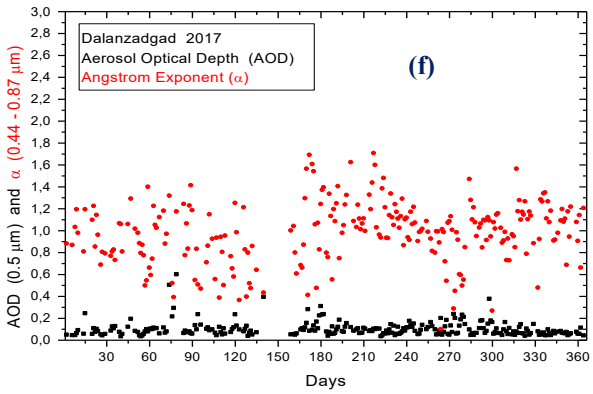

Fig. 4.Time series of AOD at $\boldsymbol{\lambda}$ = 0.5 µm (Black points) and Angstrom Exponent α at 0.44 – 0.87 µm (red points).

4.2 Single Scattering Albedo

The single scattering albedo (ω_0) is one of the optical parameters that accounts for the importance of diffusion in estimating the radiative impacts of aerosols. (ω_0) corresponds physically to the ratio between the diffusion cross section (σ_d) and the extinction cross section (σ_e) of a particle, it translates the probability that the photons intercepted by the aerosol particle are diffused and it is defined by equation 3:

$$\omega_0 = \frac{\sigma_d(\lambda)}{\sigma_e(\lambda)} = \frac{\sigma_d(\lambda)}{\sigma_a(\lambda)+\sigma_d(\lambda)} \qquad (3)$$

Where σa is the absorption cross-section of aerosol. The absorption properties are directly related to the chemical composition of the aerosol and to its refractive index. The more aerosol absorbing, the larger the imaginary part of the refractive index and the smaller ω_0. For a non-absorbing aerosol (imaginary part of the index of refraction equal to 0), ω_0 is equal to 1.

Globally, the most of the light is scattered and very little is absorbed. Daily averages of ω_0 obseved at Ouarzazate presents a wide range of variation (0.36-0.90) that indicates the polydispersion of the particles of the Saharan source and the influence of the Atlantic advections. For Dalanzadgad, the variation is small and can be explained by the distance of the source which leads to a monodispersion effect of the particles supported by the meteorological evolution conditions [25]. In general, the spectral single scattering albedo SSA, annual averages varies in the interval (0,8-0.98) indicating dominant scattering (Figure 5).

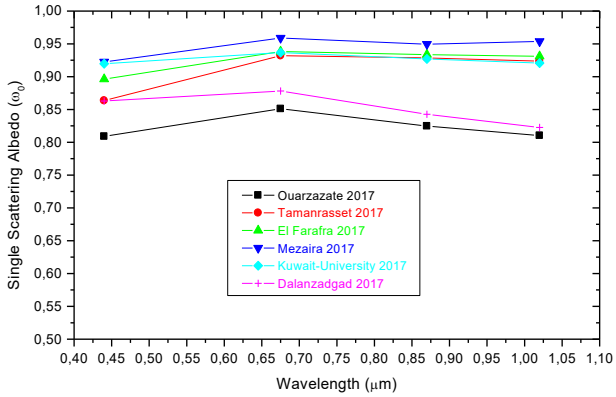

Fig.5. Annual average of SSA at SW and LW.

4.3 Aerosol Radiative Forcing

The aerosol radiative forcing (expressed in W/m^2) is defined as the difference of the net radiative flux resulting from the presence of aerosols (Equation 4). It can be quantified at the top of the atmosphere (z at the top of the TOA atmosphere) or at the ground surface (z at the BOA surface). A positive radiative forcing tends to warm the system when the negative tends to cool it:

$$\Delta F_z = (F^{\downarrow} - F^{\uparrow}) - (F^{\downarrow 0} - F^{\uparrow 0}) \qquad (4)$$

By distinguishing the flux F↑ (visible + infrared) rising and the flow F↓ (visible + infrared) descending. The indices (↑0) and (↓0) correspond to the fluxes calculated without aerosol, the case of the very clear sky. A clean aerosol-free atmosphere is characterized by a maximum of global irradiance, a minimum of diffuse irradiance and optical depth very close to zero.

Figure 6.1 shows the monthly means of ARF at surface, these are ranged from -88 W/m^2 recorded in July at Mezaira to – 9 W/m^2 observed in January at Tamanrasset and in November at El Farafrat. The negative value at surface reveals that the desert dust aerosol reduced significantly the solar radiation at the ground level producing a large surface cooling essntialy in summer. Dalanzadgad remains a special case with a weak regular variation throughout the year explained by the altitude and the remoteness of the emission sources.

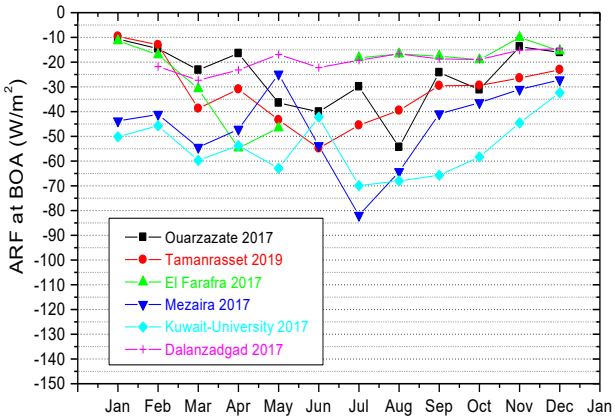

Fig.6.1 Monthly mean of ARF at surface

At top of the atmosphere given in figure 6.2, the monthly means ARF show little regular variation throughout the year ranged from -25 W/m^2 (Kuwait) to +4 W/m^2 (Tamanrasset). The passages from negative to positive values observed some times can be explained by the greater amount of the radiative energy available that has been reflected by the passenger's cirrus clouds.

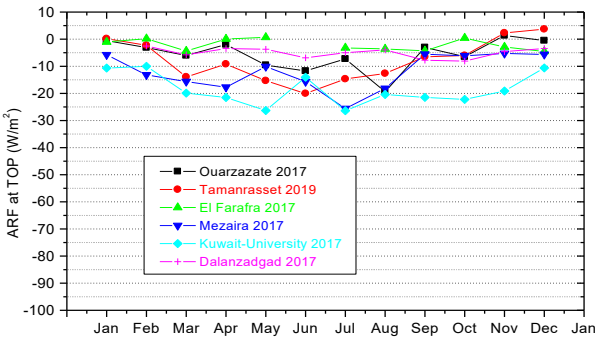

Fig.6.2 Monthly mean of ARF at top of the atmosphere.

Monthly means ARF relative to the Atmospheric column which represent the difference between the net forcing at the top and that at surface is always positive and reache the maximum of +55 W/m^2 in July at Mezaira (Figure 6.3). The curves show quite different variations from one site to another with relatively high values often in summer. This suggests a significant absorption of solar radiation in the atmosphere, leading to a significant atmospheric warming in line with the principle of conservation of energy always valid at all geographic positions.

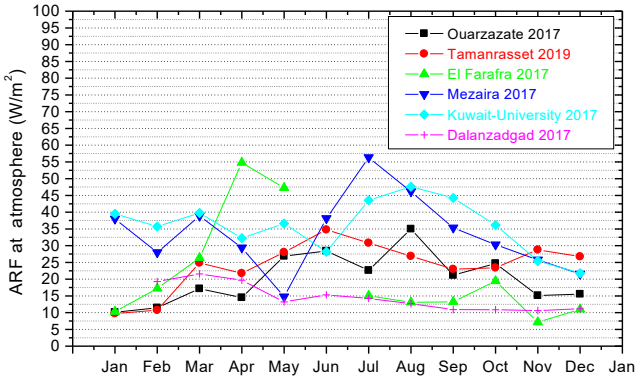

Fig.6.3. Monthly mean evolutions of aerosol radiative forcing in the atmosphere column.

5 Conclusions

The high AODs, daily averages were registred at Ouarzazate, Tamanrasset, Mezaira, Kuwait- University, confirm the influence of the desert mineral dust near and in the Saharan emission sources. Mainly in Spring and Summer we observe values higher than 0.3 except at .Dalanzadgad which represent a special case, high altitude and the remoteness of the dust emission sources are at the origine of a very weak regular variation throughout the year. Daily average of Angstrom exponent vary between 0.2 and 2.4 with a very high frequency of appearance of low values in summer especially in Tamanrasset, which characterizes the desert areas. For other sites, the frequency of appearance of large values becomes relatively high and explains the influence of fine particles particularly at El Farafra. Annual averages of the single scattering albedo varies between 0.8 and 0.98 show the importance of the scattering phenomena. The large ARF negative values of monthly average at surface (-88W/m^2 to -10 W/m^2) confirm the influence of the cooling tendencies of desert aerosol at surface, quite representative of the importance of forward scatter of the coarse particle modes characteristic of desert aerosols which cause a decrease in the net flux at the ground surface. At the top of the atmosphere ARF are essentially negatives corresponding to the increase of the flux due to the diffusion of the radiation towards the space by the aerosols contributing significantly to cooling the Earth-Atmosphere system. Positive values indicate a greater amount of radiative energy reflected by the contribution of the passenger cirrus. Monthly means ARF relative to the Atmospheric column show curves with quite different variations depending of geographic positions with always positive values that suggests a significant atmospheric warming in line with the principle of conservation of energy.

Acknowledgments

Authors want to thank all P.I of AERONET sites: Emilio Cuevas-Agullo (Ouarzazate and Tamanrasset), Mossad El-Metwally (El Farafra), Brent N Holben (Mezaira and Dalanzadgad) and Hala Khalid Al-Jassar (Kuwait-University).

References

1. I. N. Sokolik, and Toon, O.B. J. Geophys. Res., 104,9423-9444. http://dx.doi.org/10.1029/1998jd200048 (1999).
2. M. Tesche, A. Ansmann, D. Muller, D. Althausen, I. Mattis, B. Heese, V. Freudenthaler, M. Wiegner, M. Esselborn, G. Pisani and P. Knippertz. Tellus B, 61,144-164.http://dx.doi.org/10.1111/j.1600-0889.2008.00390.x (2009).
3. Y. J. Kaufman, D. Tanré et al. Nature, 419 (6903),215-223. http://dx.doi.org/10.1038/nature01091 (2002).
4. O. Dubovik and M.D. King. J. Geophys. Res., 105,20,673-20,696. http://dx.doi.org/10.1029/2000jd900282. (2000).
5. Y. Balkanski, M.Schulz, T. Claquin and S. Guibert. .Atmos.Chem. Phys, 7(1), 81-95. http://dx.doi.org/10.5194/acp-7-81-2007 (2007).
6. Y. J. Kaufman, I. Koren, L.A.Remer, D. Tanré, P. Ginoux and co-authors. J.Geophys. Res. 110. http://dx.doi.org/10.1029/2003jd004436 (2005).
7. G. R. Jeong and I. N. Sokolik. J. Geophys. Res. 112,D21308.http://dx.doi.org/10.1029/2007jd008442 (2007).
8. O. Dubovik, A. Smirnov, B. N. Holben, M. D. King, Y. J. Kaufman, T. F. Eck, I. Slutsker, J. Geophys. Res. Atmos., 105 9791-9806 (2000).
9. A. Smirnov, B. N. Holben, T. F. Eck, O. Dubovik, I. Slutsker, Remote Sens. Environ., 73(3) 337-349 (2000).
10. B. N. Holben, T. F. Eck, I. Slutsker, D. Tanré, J. P. Buis, A. Setzer, E. Vermote, J. A. Reagan, Y. J. Kaufman, T. Nakajima, F. Lavenu, I. Jankowiak, A. Smirnov, Remote Sens. Environ., 66 (1), 1-16 (1998).
11. O. Dubovik, M. D. King, J. Geophys. Res. Atmos., 105. 20673-20696 (2000).
12. M. Diouri, S. I. Sanda, CLEOPATRE-I code, J. Aerosol Sci., 28 .S459 (1997).
13. M. Wendisch, W. von Hoyningene-Huene, Atmos Environ., 28 (5) .785-792 (1994).
14. M.I. Mishchenko, L.D. Travis, A.A. Lacis, A.A, Cambridge University Press, New York (2006).
15. Ångström, A. Tellus, 22, 205–218, https://doi.org/10.3402/tellusa.v22i2.10215 (1970).
16. Shaw. G. E. Sun Photometry, B.Am.Meteorol. Soc., 64, 4-10,https://doi.org/10.1175/1520-0477(1983)064<0004:SP>2.0.CO;2 (1983).
17. B.N, Holben., Eck, T. F., Slutsker, I., Tanre, D., Buis, J. P., Setzer, A., Vermote, E., Reagan, J. A., Kaufman, Y., Nakajima, T., Lavenue, F., Jankowiak, I., and Smirnov, . Remote Sens. Environ., 66,1-16, https://doi.org/10.1016/S0034-4257(98)00031-5 (1998).
18. USNO: Approximate Solar Coordinates derived from The Astronomical Almanac, available at: http://aa.usno.navy.mil/faq/docs/SunApprox.php, last access: 1 August 2018.
19. F. Kasten and Young, A. T.Appl. Optics, 28, 4735-4738,https://doi.org/10.1364/AO.28.004735 (1989).
20. Hamonou, Chazette, E., P., Balis, D., Dulac, F., Schneider, X., Galani, E., Ancellet, G., and Papayannis, .J. Geophys. Res., 104, 22257-22270,https://doi.org/10.1029/1999JD900257 (1999).
21. Bodhaine, B. A., Wood, N. B., Dutton, E. G., and Slusser, J. R. J. Atmos. Ocean. Tech., 16, 1854-1861, https://doi.org/10.1175/1520-0426(1999)016<1854:ORODC>2.0.CO;2, (1999).
22. Komhyr, W. D., Grass, K. D., and Leonard, R. K,1962–1987, J. Geophys. Res., 94, 9847-9861, https://doi.org/10.1029/JD094iD07p09847 (1989).
23. A. Tahiri and M. Diouri. Environment, Energy and Earth Sciences E3S Web of Conferences 37 03004.https://doi.org/10.1051/e3sconf/20183703004 (2018).
24. C. Toledano et al.Tellus 61B, 216-228.Doi: 10.1111/ j.1600-0889. 2008. 00382.x (2009).
25. A. Tahiri, M. Diouri and J. Barkani. J. Mater.Environ.Sci., 2018, Vol.9, Issue 10, Page 2870-2883.http://www.jmaterenvironsci.com (2018).
26. A. Tahiri and M .Diouri. Environmental sciences,Vol.3, 2015, no.1, 17-29. HIKARI Ltd, http://dx.doi.org/10.12988/es.2015.4118.
27. D. Kim, M. Chin, H. Yu, T.F. Eck, A. Sinyuk, A. Smirnov, B. N. Holben, Atmos. Chem. Phys., 11 10733-10741 (2011).